DOI 10.5012/bkcs.2009.30.12.2962

Photodissociation Dynamics of C_2H_4BrCl: Nonadiabatic Dynamics with Intrinsic C_s Symmetry

Kyoung-Seok Lee,[†] Dababrata Paul, Kiryong Hong, Ha Na Cho, Kwang-Woo Jung,[‡,*] and Tae Kyu Kim[*]

Department of Chemistry and Center for Functional Materials, Pusan National University, Busan 609-735, Korea
[*]E-mail: tkkim@pusan.ac.kr
[†]Division of Metrology for Quality Life, Korea Research Institute of Standards and Science, Daejeon 305-340, Korea
[‡]Department of Chemistry and Institute of Nanoscience & Tech., Wonkwang University, Iksan, Chonbuk 570-749, Korea
[*]E-mail: kwjung@wonkwang.ac.kr
Received September 28, 2009, Accepted October 14, 2009

The photodissociation dynamics of 1,2-bromochloroethane (C_2H_4BrCl) was investigated near 234 nm. A two-dimensional photofragment ion-imaging technique coupled with a [2+1] resonance-enhanced multiphoton ionization scheme was utilized to obtain speed and angular distributions of the nascent Br($^2P_{3/2}$) and Br*($^2P_{1/2}$) atoms. The total translational energy distributions for the Br and Br* channels were well characterized by Gaussian functions with average translational energies of 100 and 84 kJ/mol, respectively. The recoil anisotropies for the Br and Br* channels were measured to be $\beta = 0.49 \pm 0.05$ for Br and 1.55 ± 0.05 for Br*. The relative quantum yield for Br* was found to be $\Phi_{Br^*} = 0.33 \pm 0.03$. The probability of nonadiabatic transition between A' states was estimated to be 0.46. The relevant nonadiabatic dynamics is discussed in terms of interaction between potential energy surfaces in C_s symmetry.

Key Words: Photodissociation dynamics, Alkyl halides, Curve-crossing, C_s symmetry, Ion-imaging

Introduction

Photolysis of volatile halogenated compounds generates bromine and/or chlorine atoms, which are notorious for their ozone depletion potential in the stratosphere.[1] Reactive halogen atoms and related radical exist in the troposphere can destroy ozone directly or catalytically. Recently it has been reported that the ozone depletion potential of atomic bromine could be 40 times larger than that of chlorine atom.[2] Therefore detailed investigation of photodissociation dynamics of bromine containing hydrocarbons are required to elucidate their effects in the atmosphere.[3-10]

Because CH_3X (X = Br or I) is the simplest organic halide systems, a number of experimental and theoretical studies have investigated the dynamics involved in the photodissociation following their A-band excitation. The most noteworthy conclusion drawn in these studies is that nonadiabatic curve-crossing dynamics play important role in the UV photodissociation of these molecules.[4,8,11-13] As Mulliken predicted,[14] there are three electronic states ($^1Q_1(3E)$, $^3Q_0(2A_1)$, and $^3Q_1(2E)$) responsible for A-band excitation. Among these states, only the $^3Q_0$ state diabatically correlates with the spin-orbit excited X* ($^2P_{1/2}$) channel in which the related transition dipole moment is aligned parallel to the C-X bond axis. The $^1Q_1$ and $^3Q_1$ states are correlated with the X($^2P_{3/2}$) production channel where the corresponding transitions are polarized perpendicular to the C-X bond. Although $^3Q_0 \leftarrow X$ transition carries most of oscillation strength of initial transition, the significant amount of X($^2P_{3/2}$) has been detected. This fact can be attributed to the coupling of the $^3Q_0$ state and the $^1Q_1$ state, which is invoked by symmetry reduction from C_{3v} to C_s during the photodissociation process.[4,15,16] This coupling is enhanced by symmetry-lowering vibration motions.[15,17] To better elucidate the photodissociation dynamics of organic halides, it is therefore necessary to study the photodissociation dynamics of molecules with intrinsic C_s symmetry and the related nonadiabatic interaction in the exit channels (Figure 1).

In spite of the importance of the photodissociation of molecules with C_s symmetry, this subject has not been widely investigated yet. Multihalogenated alkanes with two different halogen atoms have the lowering symmetry (C_s) than their monohalogen analogues (C_{3v}). The small numbers of theoretical[18,19] and experimental[3,5,20] efforts in this area have studied the photodissociation of bromochloromethane (CH_2BrCl). The photodissocia-

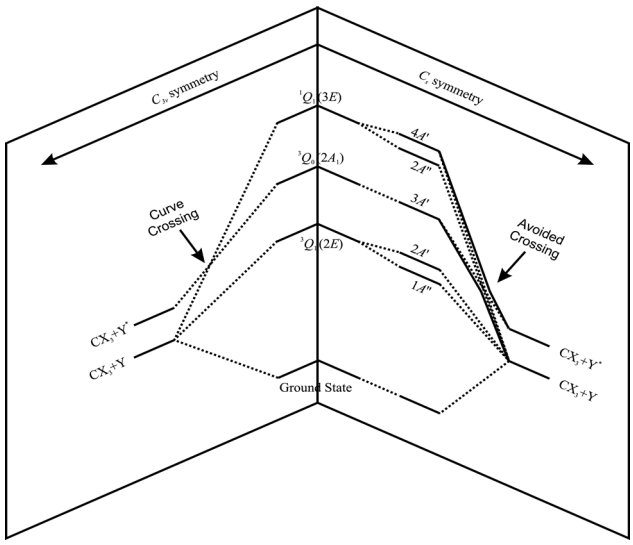

Figure 1. Schematic diagram for the photodissociation of a CX_3Y molecule. The left side represents the reaction coordinate with C_{3v} symmetry, and the right side indicates the reaction coordinate with C_s symmetry.

tion dynamics of CH_2BrCl can be explained simply in terms of potential energy surfaces in C_s symmetry, because its molecular geometry is conserved during the photodissociation process.[16] For multihalogenated alkanes with two different halogen atoms, the degenerated $^1Q_1$ and $^3Q_1$ states split into [4A', 2A''] and [2A', 1A''], respectively. The $^3Q_0$ state corresponds to the 3A' state. The 3A' and 4A' interact to form an avoided crossing which is responsible for the nonadiabatic dynamics following A-band excitation in the C_s symmetry. Though the photodissociation dynamics of 1,2-bromochloroethane (C_2H_4BrCl) in A-band was investigated by previous studies,[7,21,22] the nonadiabatic dynamics was not explained in terms of interaction between potential energy surfaces in C_s symmetry.

In the present study, we investigate the photodissociation dynamics of C_2H_4BrCl at 234 nm. The nascent Br and Br^* atoms were selectively detected using a [2+1] resonance-enhanced multiphoton ionization (REMPI) scheme. The relative quantum yield for the Br and Br^* channels were measured. Their speed and angular distributions were obtained by use of a velocity map ion-imaging technique. The results provide an insight into the photodissociation dynamics of a molecule with C_s symmetry, and can be applied to the photodissociation of other complicated multihalogenated alkanes.

Experiment

The details of experimental setup used in this study have been described elsewhere.[4,15,16] In brief, the velocity map ion-imaging spectrometer consists of supersonic molecular beam source and a time-of-flight (TOF) mass spectrometer. A pulsed valve (General valve, Series 9) with an 800 μm diameter orifice was operated synchronously with the laser pulses, typically at 10 Hz with a pulse duration of 200 μs. The molecular beam entered into the ionization region of the main chamber passing through a skimmer and pinhole with a diameter of 1 mm. Usually the sample mixture was prepared with 15 torr C_2H_4BrCl (Aldrich, 95%) seeded in 99.99% He at a stagnation pressure of ~ 1.5 atm without further purification.

Linearly polarized UV laser light was produced by doubling of the Nd:YAG laser (Spectra Physics, GCR-170) pumped dye laser (Lumonics HD 500) output using a BBO crystal and was aligned utilizing a half-wave retardation plate. The UV laser light with a typical energy of 30 - 100 μJ/pulse was focused perpendicularly onto the molecular beam in the ionization region by lens with a 250 mm focal length. A single UV laser pulse excited C_2H_4BrCl molecules and ionized resultant Br and Br^* fragments. The [2+1] REMPI technique employed to selectively ionize Br (233.7 nm, *via* 6p $^4P_{3/2}$ intermediate state) and Br^* (234.0 nm, *via* the intermediate state of 6p $^4D_{1/2}$).[23,24]

The resultant Br and Br^* ion clouds were accelerated and focused by an electrostatic lens to create an image onto a two dimensional position sensitive detector.[25] This detector is composed of a dual chevron microchannel plate (MCP), a phosphor screen (Galileo Electrooptic Corp. 3040FM), an image intensifier was triggered by a pulse at a certain delay to segregate the signals of Br^+ ions from those of scattered light and other ions with different masses. Over 10000 shots were averaged to construct each image while the laser frequency was scanned repeatedly across the Doppler profile of the relevant Br/Br^* transition. In order to remove the background, an image was obtained at an off-resonance wavelength under the same conditions and subtracted from the image of the Br fragments. TOF spectra were obtained using a photomultiplier tube (Hamamatsu, 1P21) instead of the charge coupled device camera.

Results and Analysis

Raw Images. The raw images of the fragments represent two-dimensional projections of the genuine three-dimensional speed/angular distributions. The raw images of Br and Br^* obtained from the photolysis of C_2H_4BrCl at 234 nm are presented in Figure 2(a) and 2(b), respectively. Inverse Abel transformation was performed to reconstruct the three dimensional velocity distributions of Br and Br^* which are cylindrically symmetric around the polarization axis of the photolysis laser beam.[26] This transformation is very sensitive to the noise, and therefore the raw images were smoothed in advance using a Gaussian filter with a 5 × 5 pixel window.[26] It is evident in Figure 2 that the image of Br^* from C_2H_4BrCl shows relatively high contributions from parallel transitions while the image of Br shows mixed distributions from both parallel and perpendicular transitions. In addition, the broad structures in the images are indicative of broad translational energy distributions.

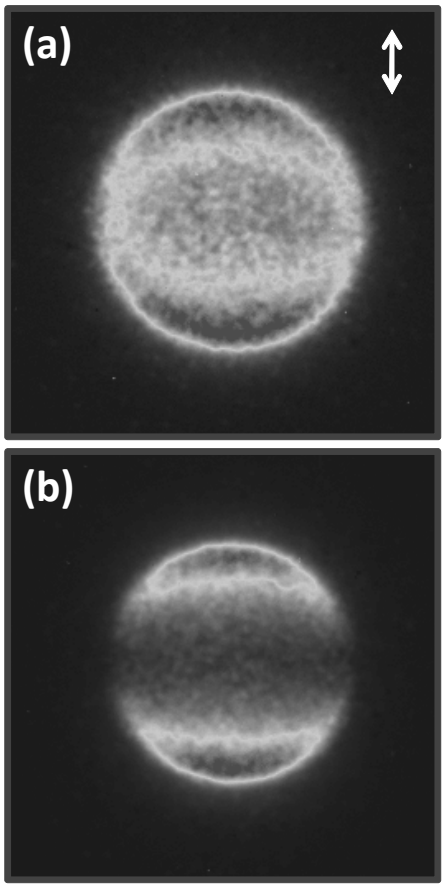

Figure 2. Raw ion images of (a) Br and (b) Br^* from the photodissociation of C_2H_4BrCl at 234 nm. The polarization vector of the laser pulse is vertically aligned.

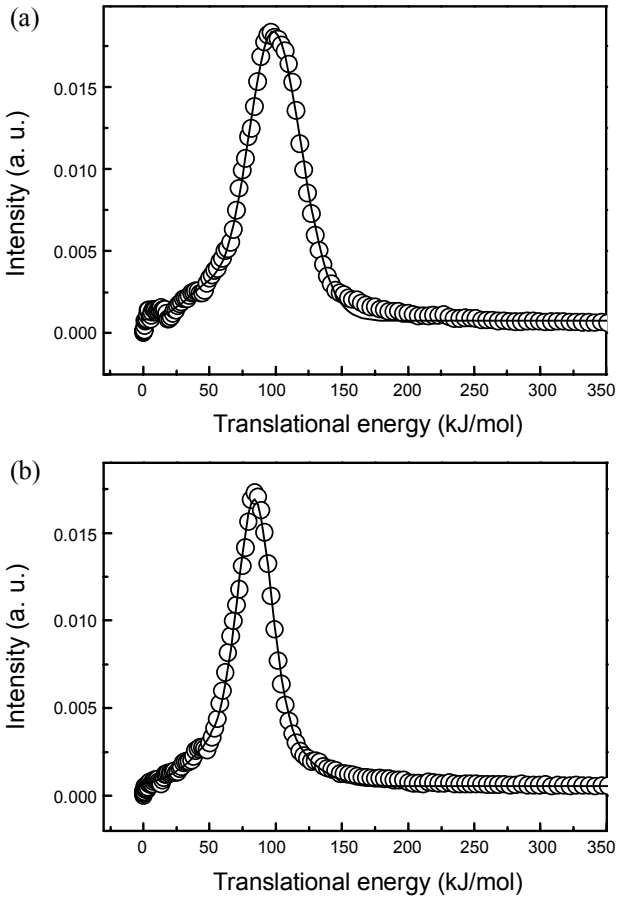

Figure 3. Total energy distributions for (a) Br and (b) Br^* pathways. The solid lines indicate the curves fitted with a Gaussian-shaped function.

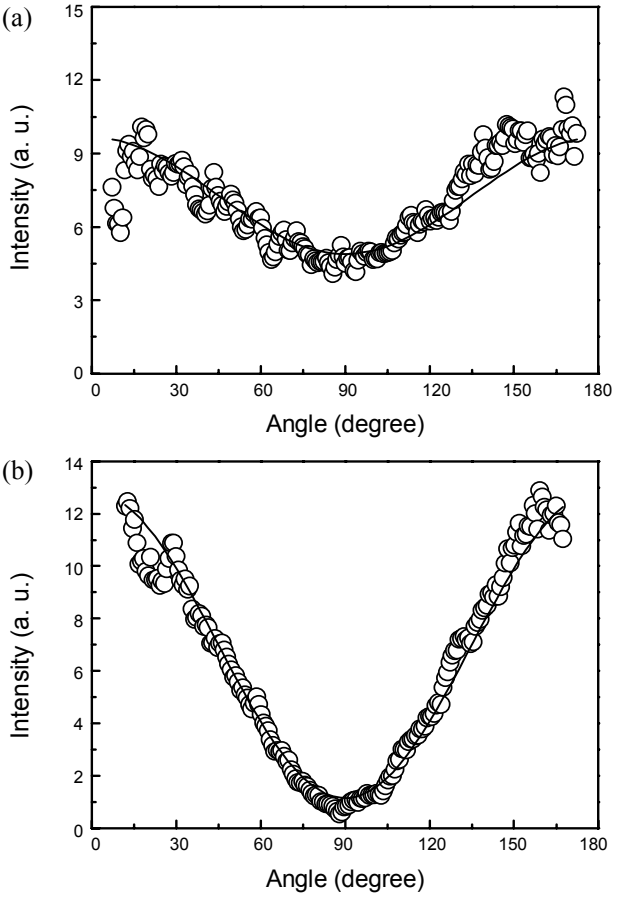

Figure 4. Angular distributions for (a) Br and (b) Br^* channels in the photodissociation of C_2H_4BrCl at 234 nm. The solid lines indicate the curve-fits with (a) $\beta = 0.49$ and (b) $\beta = 1.55$.

Translational Energy Distributions. A speed distribution, $P(v)$, was extracted by integration of a reconstructed three-dimensional velocity distribution over all angles at each speed. The center-of-mass translational energy distribution, $P(E)$, was obtained *via* conversion of the speed distribution using the simple relationship:

$$P(E) = P(v)\frac{dv}{dE} \propto \frac{P(v)}{v}, \quad (1)$$

$$E_T = \frac{1}{2}\left(m_{Br} + m_{C_2H_4Cl}\right)\left(\frac{m_{Br}}{m_{C_2H_4Cl}}\right)v_{Br}^2. \quad (2)$$

The translational energy was calibrated using the translational energies of Br and Br^* following the photolysis of diatomic HBr and Br_2 under the same conditions.

The total translational energy distributions are displayed in Figure 3(a) for the Br channel and Figure 3(b) for the Br^* channel. Each distribution in Figure 3 was well fitted by a *single* Gaussian distribution, indicating that the bromine fragments are produced *via* direct dissociation on the repulsive surfaces. The broad feature of the distribution in Figure 3(a), as well as the oscillatory feature shown in the low energy shoulder, may indicate that vibrational excitation of the C_2H_4Cl radical is involved in the photodissociation process. The average translation energy, $\langle E_T \rangle$, for the Br channel was found to be 99.8 kJ/mol.[22] The Gaussian-shaped translational energy distribution is characterized by a width of 42.9 kJ/mol. To calculate the fraction of the translational energy of Br to the available energy (f_T), the

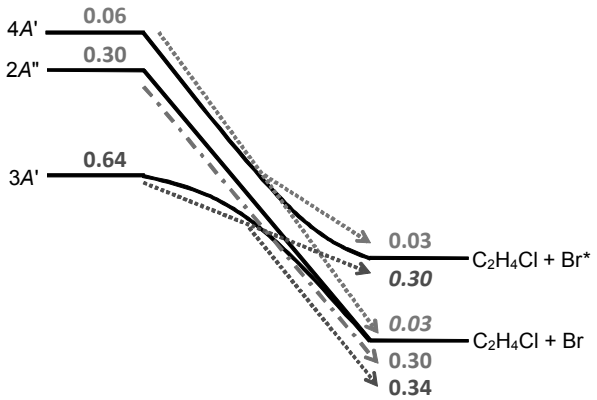

Figure 5. Schematic diagram of the photolysis of C_2H_4BrCl on the $3A'$ ($^3Q_0$) and [$4A'$, $2A''$] ($^1Q_1$) surfaces. Dotted and dash-and-dot lines schematically show the trajectories along individual pathways. The numbers in italics represent the fraction of molecules dissociating *via* nonadiabatic curve crossing.

Table 1. Available energies, average translational energies, energy fractions, recoil anisotropy parameters, and relative quantum yields of Br and Br* resulting from the photolysis of C_2H_4BrCl at 234 nm. The energy unit is kJ/mol. f_T is the fraction of the translational energy to the available energy measured in this work. Numbers in parentheses are the errors corresponding to one standard deviation.

Channel	$h\nu$	E_{avl}	$\langle E_T \rangle$	FWHM	f_T	β	Φ
$C_2H_4Cl + Br$	511.9	219.0	99.8	44.1	0.46	0.49(0.05)	0.67(0.03)
$C_2H_4Cl + Br^*$	511.1	174.2	84.4	30.0	0.49	1.55(0.05)	0.33(0.03)

following relationship was used:

$$f_T = \frac{\langle E_T \rangle}{E_{avl}} \tag{3}$$

$$E_{avl} = h\nu - D_0 - E_{el} + E_{int} \tag{4}$$

where E_{avl} and $h\nu$ designates the available energy of the photodissociation and the photon energy of 234 nm, respectively. The parameter D_0 indicates the dissociation energy of the C-Br bond; a value of D_0 = 294.0 kJ/mol was chosen from the literature.[21] The electronic energy, E_{el}, is equal to the appropriate electronic energy level of atomic bromine, and was chosen to be 0 for the ground state Br and 44.1 kJ/mol for the excited state Br*. Because rotational and vibrational excitations are negligible in a supersonic molecular beam, the internal energy of C_2H_4BrCl, E_{int}, was set to zero. Using the values outlined previously, a value of f_T = 0.46 was determined for the Br channel.

In the translational energy distribution for the Br* channel [Figure 3(b)], the oscillatory structure is not easily seen and a narrower translational energy distribution is observed. Although experimental limitations prohibited further resolution of the fine structures shown in Figure 3, work is currently under way to construct an imaging system capable of more precise measurement. The average translational energy ($\langle E_T \rangle$) was found to be 84.4 kJ/mol. The full width at half maximum (FWHM) of the distribution is 30.0 kJ/mol, which is much lower than that of the Br channel. The fraction of the translational energy to the available energy (f_T) was found to be 0.49.

Recoil Anisotropies and Relative Quantum Yields. The angular distribution of the fragments, $P(\theta)$, was extracted by integrating a reconstructed three-dimensional velocity distribution over an appropriate range of speed at each angle. The parameter θ indicates the angle between the laser polarization axis and the recoil axis of the bromine fragments (that is bond axis of C-Br bond). The angular distributions of Br and Br* are presented in Figure 4. The angular distribution can be characterized by the anisotropy parameter β using

$$P(\theta) = 1 + \beta P_2(\cos\theta), \tag{5}$$

where P_2 (cos θ) is a second-order Legendre polynomial.[27] Fitting the plots in Figure 4 with the standard formula $\beta = 0.49 \pm 0.05$ for Br and $\beta = 1.55 \pm 0.05$ for Br*. It should be mentioned that our recoil anisotropy values are significantly smaller than those in previous study.[7]

The relative quantum yields are defined as follows:

$$\Phi_{Br} = \frac{N_{Br}}{N_{Br} + N_{Br^*}}, \tag{6}$$

$$\Phi_{Br^*} = 1 - \Phi_{Br}, \tag{7}$$

where N_X is the number of species X (X = Br, Br*). These numbers were extracted from the relative [2+1] REMPI ion signal intensities of Br and Br* in the TOF spectra, yielding values of $\Phi_{Br} = 0.67 \pm 0.03$ and $\Phi_{Br^*} = 0.33 \pm 0.03$. The extracted experimental parameters are listed in Table 1.

Discussion

In the UV absorption spectrum of C_2H_4BrCl, the broad peak with a maximum near 200 nm corresponds to the $\sigma^* \leftarrow n$. transition localized on the C-Br bond. The second peak arises at 195 nm which is presumably due to the $\sigma^* \leftarrow n$ transition of the C-Cl bond. The absorption spectrum of C_2H_4BrCl is very similar with that of CH_3Br between 195 nm and 280 nm and quite close to the CH_3Cl below 195 nm.[28,29] This indicates that the electronic transitions of the two chromophores and the dynamics associated with the halogen forming channels could be considered independently as in the case of CH_2BrCl.[5] This fact also can be confirmed by our experimental observations. In the Figure 3, translational energy distributions for Br and Br* fragments were well fitted by a single Gaussian distribution, indicating that the bromine fragments are produced *via* direct dissociation on the repulsive surfaces. It has been shown that Cl formation from 234 nm photodissociation of CH_2BrCl mainly arises from secondary process of CH_2Cl radical.[7,22]

The recoil anisotropy parameters observed in this study ($\beta = 0.49 \pm 0.05$ for Br and $\beta = 1.55 \pm 0.05$ for Br*) are less than the limiting value of parallel transition ($\beta_{lim}^{\parallel} = +2$), indicating that both perpendicular and parallel transitions are responsible for generation of Br and Br*. The potential energy surfaces of C_2H_4BrCl can be inferred from those of CH_2BrCl. The structural similarity of the two molecules leads us to expect these molecules to have similar potential energy surfaces pertinent to the *A*-band excitation in the UV region, except for slight differences in oscillating strengths and energies of the individual states.[5] The *A*-band absorption of CH_3Br with intrinsic C_{3v} symmetry was predicted by Mulliken to stem from a $\sigma^* \leftarrow n$ type of electronic transition.[14,30] In Mulliken's notation, the three optically accessible states of CH_3Br are denoted $^1Q_1$, $^3Q_0$, and $^3Q_1$, in descending order of energy by analogy with the $^1\Pi_1$, $^3\Pi_0^+$, and $^3\Pi_1$ components of HBr. As discussed, in molecules with intrinsic C_s symmetry such as CH_2BrCl, the $^3Q_1$ state is splits into the 2*A*'

Table 2. Possible pathways for Br and Br* production via the 234 nm photodissociation of C_2H_4BrCl. The pathways without nonadiabatic transition, $3A' \leftarrow 3A'$, $2A'' \leftarrow 2A''$, and $4A' \leftarrow 4A'$ are abbreviated for simplicity to $3A'$, $2A''$, and $4A'$.

Product	Pathways	
	without nonadiabatic transition	*via* nonadiabatic transition
Br	$3A'$, $2A''$	$3A' \leftarrow 4A'$
Br*	$4A'$	$4A' \leftarrow 3A'$

Table 3. Fractions of molecules dissociating via individual pathways and curve-crossing probabilities.

$C_{Br}^{\parallel}$	$C_{Br}^{\perp}$	$C_{Br^*}^{\parallel}$	$C_{Br^*}^{\perp}$	$f_{3A'\leftarrow 3A'}$	$f_{3A'\leftarrow 4A'} + f_{2A''\leftarrow 2A''}$	$f_{4A'\leftarrow 4A'}$	$f_{4A'\leftarrow 3A'}$	P_{up}	P_{down}
0.52	0.48	0.91	0.09	0.35	0.32	0.03	0.30	0.46	≤ 0.92

and $1A''$ states. The $^3Q_0$ state does not split and is directly correlated with the $3A'$ state. The $^1Q_1$ state is correlated with the $4A'$ and $2A''$ states in the C_s symmetry. In the UV spectrum of CH_2BrCl, the absorption band of lowest [$2A'$, $1A''$] ($^3Q_1$) states is shifted to significant longer wavelengths compared to the $^3Q_1$ state of CH_3Br. Another feature is that the $3A'$ ($^3Q_0$) and [$4A'$ and $2A''$] ($^1Q_1$) states are very close and have nearly equal widths for CH_2BrCl.[5] Because C_2H_4BrCl is also of intrinsic C_s symmetry, the potential energy surfaces reached *via* the transition localized on the C-Br bond seem to be similar to those of CH_2BrCl. Therefore the $3A'$ ($^3Q_0$) and [$4A'$ and $2A''$] ($^1Q_1$) states are accessible at 234 nm excitation. The $4A'$ and $2A''$ states are responsible for the electronic transitions aligned perpendicular to the C-Br bond and correlate with the channel for Br formation, whereas the $3A' \leftarrow 1A'$ transition is polarized parallel to the bond and correlates with the Br* channel.[16] However, in C_s symmetry, an avoided crossing can be formed between the $3A'$ and $4A'$ surfaces. As a consequence, 234 nm excitation of C_2H_4BrCl leads to Br production *via* three pathways ($3A'$, $2A''$, and a nonadiabatic transition from $4A'$ to $3A'$), and to Br* production *via* two pathways ($4A'$ and a nonadiabatic transition from $3A'$ to $4A'$). The nonadiabatic transition from the $3A'$ to $4A'$ results in the generation of the parallel component for the Br* channel. Moreover the nonadiabatic transition from the $4A'$ to $3A'$ results in the generation of the perpendicular observed for the Br channel. All possible pathways responsible for Br and Br* production channels are listed in Table 2.

The relative contributions of the parallel and perpendicular transitions to the obtained anisotropy parameters can be calculated from the following relationship:

$$\begin{pmatrix} \beta_{Br} \\ \beta_{Br^*} \end{pmatrix} = \begin{pmatrix} C_{Br}^{\parallel} & C_{Br}^{\perp} \\ C_{Br^*}^{\parallel} & C_{Br^*}^{\perp} \end{pmatrix} \begin{pmatrix} \beta_{lim}^{\parallel} \\ \beta_{lim}^{\perp} \end{pmatrix} \tag{8}$$

where C_N^M ($M = \perp, \parallel$; N = Br, Br*; $C_N^{\perp} + C_N^{\parallel} = 1$) is the relative fraction of the species N generated by either the parallel ($\parallel$) or perpendicular ($\perp$) transition. $\beta_{lim}^{\parallel}$ and $\beta_{lim}^{\perp}$ are the limit values of the anisotropy parameters for the parallel and perpendicular transitions, respectively. As mentioned before, the electronic transition of C_2H_4BrCl at 234 nm is a $\sigma^* \leftarrow n$ transition mainly localized on the C-Br bond. Therefore, a limiting value for the parallel transition can be deduced from that of the Br* generated in the 234 nm photodissociation of CF_3Br.[15] It has been known that only $^3Q_0$ (pure parallel component) is responsible for the generation of Br* in the photodissociation of CF_3Br at 234 nm. As a result, $\beta_{lim}^{\parallel} = 1.8$ was chosen for the analysis. On the same account, $\beta_{lim}^{\perp} = -\frac{1}{2}\ \beta_{lim}^{\parallel} = -0.9$ was selected. The use of limiting values is not rigorous for repulsive dissociation of polyatomic molecule, especially when a significant fraction of energy appears in internal energy of fragment.[31] Nevertheless, this approach helps one to interpret the data qualitatively and discuss the related dynamic processes during photodissociation. The fractions of the dissociation pathways leading to the generation of the parallel and perpendicular components of Br and Br* have been extracted using following relationship:

$$\begin{pmatrix} \Phi_{Br} C_{Br}^{\parallel} & \Phi_{Br} C_{Br}^{\perp} \\ \Phi_{Br^*} C_{Br^*}^{\parallel} & \Phi_{Br^*} C_{Br^*}^{\perp} \end{pmatrix} = \begin{pmatrix} f_{3A'\leftarrow 3A'} & f_{3A'\leftarrow 4A'} + f_{2A''\leftarrow 2A''} \\ f_{4A'\leftarrow 3A'} & f_{4A'\leftarrow 4A'} \end{pmatrix} \tag{9}$$

where $f_{A\leftarrow B}\left(A, B = 3A', 4A', 2A''\right)$ is the fraction of molecules that dissociate *via* the A and B surfaces before and after the crossing point, respectively, and $\sum_{A,B} f_{A\leftarrow B} = 1$. Then the curve-crossing probability were calculated using,

$$\begin{aligned} P_{up} &= \frac{f_{4A'\leftarrow 3A'}}{f_{4A'\leftarrow 3A'} + f_{3A'\leftarrow 3A'}} \\ P_{down} &= \frac{f_{3A'\leftarrow 4A'}}{f_{4A'\leftarrow 4A'} + f_{3A'\leftarrow 4A'}} \leq \frac{f_{3A'\leftarrow 4A'} + f_{2A''\leftarrow 2A''}}{f_{4A'\leftarrow 4A'} + f_{3A'\leftarrow 4A'} + f_{2A''\leftarrow 2A''}} \end{aligned} \tag{10}$$

where P_{up} and P_{down} are probability of nonadiabatic transitions from the lower to the upper and from the upper and the lower surfaces, respectively. The resultant fractions and curve crossing probabilities are listed in Table 3.

The nonadiabatic curve crossing probability, P, may be estimated by using a one-dimensional Landau-Zener equation:

$$P = \exp\left(-\frac{\xi}{\upsilon}\right) \tag{11}$$

where ξ is an adjustable parameter dependent on the splitting between adiabatic surfaces and the difference in the slopes of the potential surfaces at the avoided crossing, and υ is the radial velocity at the avoided crossing point.[32,33] Although the Landau-

Zener model ignores several internal degrees of freedom that may play important role in the photodissociation process, its application provides qualitative understanding of the nonadiabatic dynamics.[15] According to this model, the curve-crossing probability monotonically decreases with v. In photodissociation of CF_3I at 248 and 304 nm,[33,34] qualitative agreement was found between this model and the experimental findings ($P_{down} = 0.035$ at 304 nm and 0.4 at 248 nm). In the case of C_2H_4BrCl, however, this model is not in agreement with the experimental findings. $P_{up} = 0.46$ and $P_{down} \leq 0.92$ (hence 0.92 is the upper limit of P_{down}) may be indicative of the difference between the up and down crossing probabilities, which is contrary to this model. Similar results have been observed for the dissociations of CH_3Br and CH_3I, in which the difference between the up and down crossing probabilities was attributed to the symmetry reduction from C_{3v} to C_s caused by zero-point motion along e-symmetry modes or the excitation of vibrational bending modes.[35,36] However in the photodissociation of C_2H_4BrCl at 234 nm, the symmetry (C_s) of the molecule is retained during dissociation process and the up and down crossing probability should be the same. Assuming the two probabilities are equal, the fraction of molecules dissociating along the $2A''$ surface was calculated to be $f_{2A''\leftarrow 2A''} = 0.30$. The values of $f_{2A''\leftarrow 2A''}$ were estimated to be 0.19 and 0.05 for CH_2BrCl and CH_3COBr, respectively.[5,16] The fraction of molecules on $2A''$ surface in the 234 nm C_2H_4BrCl photodissociation is considerably larger than those in the photodissociation of molecules with C_s symmetry.

It is interesting to compare shapes of upper and lower surfaces. The difference in FWHM between the two total translational energy distributions (Figure 3, FWHM = 44.1 kJ/mol for Br and 30.0 kJ/mol for Br^* pathways) may be caused by the difference in shape between the upper and lower surfaces. It has been shown in an *ab initio* and trajectory study[17,36] of A-band photodissociation of CH_3I that the $^1Q_1$ surface has a small bending force constant, which is considered to induce the symmetry reduction outside the conical intersection. It was also found that the $^3Q_0$ surface retains a large bending vibrational force constant even outside the conical intersection. This feature leads to the damping of the vibrational motion of CH_3. Consequently, the transition from the $^3Q_0$ to $^1Q_1$ surface conserves the vibration which is initially excited after photodissociation commences, whereas the transition from the $^1Q_1$ to $^3Q_0$ surface reduces the vibrational excitation. Therefore as the fraction of the $^1Q_1 \leftarrow {}^3Q_0$ becomes larger, more vibrational excitation is expected. This relationship between the vibrational excitation of fragments and the shape of the relevant potential energy surfaces can be applied to the case of C_2H_4BrCl. In the photodissociation of C_2H_4BrCl at 234 nm, 52% of Br atoms originate from the parallel transition, indicating that this fraction of Br atoms originates from molecules dissociating on the lower $3A'$ ($^3Q_0$) surface, without a nonadiabatic transition. Contrary, the majority (91%) of Br^* atoms arise from molecules dissociating on the upper $4A'$ ($^1Q_1$) surface after nonadiabatic transition from the lower $3A'$ ($^3Q_0$) surface. Remembering that the total translational energy distribution for Br forming channel is much broader, it can be concluded that the vibration excitation induced by the recoil impulse are retained due to the small vibrational force constants when molecules dissociate on the $3A'$ ($^3Q_0$) surface without nonadiabatic transition. The broad translational energy distributions as well as the oscillatory structure observed in the low energy regions of the distributions are also indicating the vibrational excitation during the photodissociation of C_2H_4BrCl. The oscillatory structure is seen more easily for the Br channel than for Br^* channel. Although the distributions cannot be resolved completely, the broadness and the oscillatory structure of the total translational energy distribution for Br channel may provide a picture for the dynamics of the vibrational excitation of fragment as described above. It is interesting fact that the parent molecule exists as a mixture of *anti* and *gauche* conformers with the former the more stable at room temperature.[37] However, the parent molecules of *anti* form remain predominantly in the molecular beam conditions.[37] We believe that the results presented here are mostly originated from the photodissociation of *anti*-C_2H_4BrCl at 234 nm.

Summary

In this work, the photodissociation dynamics of C_2H_4BrCl has been investigated at 234nm utilizing a photofragment ion-imaging technique coupled with a REMPI scheme. The nascent Br and Br^* atoms were detected after C-Br dissociation *via* the $\sigma^* \leftarrow n$ transition localized on the C-Br bond. The total translational energy distributions for Br and Br^* channels was found to be well modeled by single Gaussian distribution. This suggests that the bromine fragments generated from direct dissociation on the repulsive surfaces without any interference of C-Cl chromophore. Based on the recoil anisotropy parameters and relative quantum yields, the relative contributions of the parallel and perpendicular transitions to the generation of bromine fragments have been extracted for the Br and Br^* channels. Using these values, the fractions of the dissociation pathways leading to the generation of the parallel and perpendicular components of Br and Br^* have been calculated. The nonadiabatic transition probability between the $3A'$ and $4A'$ potential energy surfaces was found to be 0.46. It is suggested that the different widths and the oscillatory structures of the translational energy distributions of Br channel may be due to the different shapes of the $3A'$ ($^3Q_0$) and $4A'$ ($^1Q_1$) surface after nonadiabatic transition. In order to better describe the nonadiabatic transition during photodissociation of molecule of C_s symmetry, we are currently investigating the photodissociation dynamics of other molecules of C_s symmetry at various photolysis wavelengths.

Acknowledgments. This work was supported by the Grant No. R-01-2008-000-20717-0 of the Basic Research Program of the Korea Science and Engineering Foundation, Republic of Korea.

References

1. Molina, M. J.; Rowland, F. S. *Nature* **1974**, *248*, 810.
2. Garcia, R. R.; Solomon, S. *J. Geophys. Res.* **1994**, *99*, 12937.
3. Tzeng, W. B.; Lee, Y. R.; Lin, S. M. *Chem. Phys. Lett.* **1994**, *227*, 467.
4. Kim, T. K.; Lee, K. W.; Lee, K. S.; Lee, E. K.; Jung, K. H. *Chem. Phys. Lett.* **2007**, *446*, 31.
5. Zou, P.; McGiven, W. S.; North, S. W. *Phys. Chem. Chem. Phys.*

2000, *2*, 3785.
6. Blanchet, V.; Samartzis, P. S.; Wodtke, A. M. *J. Chem. Phys.* **2009**, *130*, 034304.
7. Hua, L.; Shen, H.; Zhang, C.; Cao, Z.; Zhang, B. *Chem. Phys. Lett.* **2008**, *460*, 50.
8. Lee, K. S.; Lee, K. W.; Lee, S. K.; Jung, K. H.; Kim, T. K. *J. Mol. Spectra.* **2008**, *249*, 43.
9. Sohn, Y.; White, J. M. *Bull. Korean Chem. Soc.* **2009**, *30*, 1470.
10. Park, J.; Lee, J.; Sim, K.; Han, J. W.; Yi, W. *Bull. Korean Chem. Soc.* **2008**, *29*, 177.
11. Eppink, A. T. J. B.; Parker, D. H. *J. Chem. Phys.* **1999**, *110*, 832.
12. Eppink, A. T. J. B.; Parker, D. H. *J. Chem. Phys.* **1998**, *109*, 4758.
13. Gougousi, T.; Samartzis, P. S.; Kitsopoulos, *J. Chem. Phys.* **1998**, *108*, 5742.
14. Mulliken, R. S. *J. Chem. Phys.* **1940**, *8*, 382.
15. Kim, T. K.; Park, M. S.; Lee, K. W.; Jung, K. H. *J. Chem. Phys.* **2001**, *115*, 10745.
16. Lee, K. W.; Jee, Y. J.; Jung, K. H. *J. Chem. Phys.* **2002**, *115*, 4490.
17. Amatatsu, Y.; Yabushita, S.; Morokuma, K. *J. Chem. Phys.* **1996**, *104*, 9783.
18. Rozonyi, T.; Gonzalez, L. *J. Phys. Chem. A* **2008**, *112*, 5573.
19. Rozonyi, T.; Gonzalez, L. *J. Phys. Chem. A* **2006**, *110*, 10251.
20. Zhou, J.; Lau, K. C.; Hassanein, E.; Xu, H.; Tian, S. X.; Jones, B.; Ng, C. Y. *J. Chem. Phys.* **2006**, *124*, 034309.
21. Lee, Y. R.; Chen, C. C.; Lin, S. M. *J. Chem. Phys.* **2004**, *120*, 1223.
22. Wang, G. J.; Zhang, H.; Zhu, R. S.; Han, K. L.; He, G. Z.; Lou, N. Q. *Chem. Phys.* **1999**, *241*, 213.
23. Park, M. S.; Jung, Y. J.; Lee, S. H.; Kim, D. C.; Jung, K. H. *Chem. Phys. Lett.* **2000**, *322*, 429.
24. NIST Atomic Spectra Database: http://physics.nist.gov/cgi-bin/AtData/main_asd.
25. Eppink, A. T. J. B.; Parker, D. H. *Rev. Sci. Instrum.* **1997**, *68*, 3477.
26. Hansen, E. W.; Law, P. L. *J. Opt. Soc. Am. A* **1985**, *2*, 510.
27. Zare, R. N.; Herschbach, D. R. *Proc. IEEE* **1963**, *51*, 173.
28. Orkin, V. L.; Khanaganov, V. G.; Guschin, A. G.; Huie, R. E.; Kurylo, M. J. *J. Phys. Chem. A* **1997**, *101*, 9224.
29. Hirayama, K. *Handbook of Ultraviolet and Visible Absorption Spectra of Organic Compounds*; Plenum Press Data Division, New York, 1967.
30. Mulliken, R. S. *J. Chem. Phys.* **1935**, *3*, 513.
31. McGiven, W. S.; Li, R.; Zou, P. ; North, S. W. *J. Chem. Phys.* **1999**, *111*, 5771.
32. Landau, L. D.; Lifshitz, E. M. *Quantum Mechanics 3*; Pergamon: New York, 1997.
33. Felder, P. *Chem. Phys.* **1991**, *155*, 435.
34. Felder, P. *Chem. Phys. Lett.* **1992**, *197*, 425.
35. Underwood, J. G.; Powis, I. *Phys. Chem. Chem. Phys.* **2000**, *2*, 747.
36. Amatatsu, Y.; Morokuma, K. *J. Chem. Phys.* **1991**, *94*, 4858.
37. Huang, J.; Hedberg, K. *J. Am. Chem. Soc.* **1990**, *112*, 2070.